

Discrete-time Contraction-based Control of Nonlinear Systems with Parametric Uncertainties using Neural Networks

Lai Wei, Ryan McCloy, and Jie Bao

Abstract—Flexible manufacturing in the process industry requires control systems to achieve time-varying setpoints (e.g., product specifications) based on market demand. Contraction theory provides a useful framework for reference-independent system analysis and tracking control for nonlinear systems. However, the determination of the control contraction metrics and control laws can be very difficult for general nonlinear systems. This work develops an approach to discrete-time contraction analysis and control using neural networks. The methodology involves training a neural network to learn a contraction metric and feedback gain. The resulting contraction-based controller embeds the trained neural network and is capable of achieving efficient tracking of time-varying references, with a full range of model uncertainty, without the need for controller structure redesign. This is a robust approach that can deal with bounded parametric uncertainties in the process model, which are commonly encountered in industrial (chemical) processes. Simulation examples are provided to illustrate the above approach.

Index Terms—Neural networks; nonlinear control; reference independent control; contraction theory; parametric uncertainties; discrete-time control contraction metric

I. INTRODUCTION

THE process industry has seen increasing variability in market demand, with time varying diversity and quantity of products. As an example, there is a trend for produce-to-order operations in polymer [1] and fine chemicals sectors. Variations are also evident in the specifications and supply volume of “raw” materials and energy (e.g., electricity). Consequently, businesses in the process industry are required to have the flexibility to dynamically adjust the volume and specifications of products, and deal with diverse sources of raw materials to remain competitive [2]. Traditionally, a chemical plant is designed and operated at a certain steady-state operating condition where the plant economy is optimized. The process industry is shifting from the traditional mass production to more agile, cost-effective and dynamic process operation closer to the market, which is the main driver for next-generation “smart plants”. As such, the control system needs to have the flexibility to drive a process to any required time-varying operational target (setpoint) to meet the dynamic market demand.

Lai Wei, Ryan McCloy and Jie Bao are with the School of Chemical Engineering, The University of New South Wales, Sydney, NSW 2052, Australia. E-mail: lai.wei1@unsw.edu.au, r.mccloy@unsw.edu.au and j.bao@unsw.edu.au (corresponding author).

This project is supported by Australian Research Council Discovery Projects DP180101717.

As most chemical processes are inherently nonlinear, flexible process operation warrants nonlinear control as the target operating conditions may need to vary significantly to minimize the economic cost. Existing nonlinear control methods, e.g., Lyapunov-based approaches, typically require redesigning the control Lyapunov function and controller when the target equilibrium changes, not suitable for flexible process operation with time varying targets. This has motivated the increasing interests and applications of contraction theory-based nonlinear control [3], [4]. Pioneered by Lohmiller and Slotine [5], contraction theory provides an approach to stability analysis and control of nonlinear systems to track arbitrary time-varying (feasible) references without redesigning the control algorithm [6], [7]. Using both the nonlinear process model and the corresponding differential dynamics, contraction theory can be used to analyze the incremental stability/contraction of nonlinear systems, and jointly synthesize a controller that ensures offset-free tracking of feasible target trajectories using control contraction metrics (or CCMs, see, e.g., [6]).

There are a number of challenges in applying contraction-based control: (1) The CCMs are often difficult to determine. The existing approaches are largely limited to polynomial systems, where CCMs can be synthesized by solving a state-dependent linear matrix inequality problem using Sum-of-Squares (SoS) programming (see, e.g., [6], [8], [9]) or RKHS theory [10]. The degree and structure of the SoS polynomials also play a critical role in determining whether a solution can be found, which for higher order systems and polynomial approximations compounds the computational burden significantly (both offline during the initial search, and online, to reconstruct the control law using geodesics); (2) Despite the discrete-time nature of modern process control systems [11], developments of tools for analyzing, designing, and implementing contraction-based control for discrete-time nonlinear systems is scarce (see, e.g. [12]), whereby continuous-time results are often applied by making assumptions as to the negligible effect of the dynamics in between discrete samples, resulting in an *ad-hoc* formulation when considering optimality (see, e.g., [4]); (3) Model uncertainties are inherent in process models. The parameters of these models are often uncertain within known ranges, which warrants robust control designs. Existing approaches for the synthesis of CCMs (see, e.g., [13]) and design of robust controllers (see, e.g., [8], [9]) are very limited when considering modeling uncertainty.

Neural networks have been used for nonlinear process modeling (e.g., [14], [15]) due to their ability to univer-

sally approximate arbitrary functions [16], finding utilization in model-based control designs, such as model predictive control (MPC) (see, e.g., [17]–[19]). Neural networks have also been effectively used in learning control and adaptive control applications [20]. A wide variety of neural network structures are available (e.g., autoencoder [21], long short-term memory (LSTM) [22], transformer [23], and Siamese network [24]), of which can greatly impact the performance of the trained neural network. However, stability design for neural network-based control is still an open problem. In particular, there are very few results on setpoint-independent nonlinear control, especially when considering (embedding) the neural network within the closed-loop control system. One solution is to develop a neural network-based control approach, using process models with uncertainty, which can be readily obtained for practical systems [25]. Compared with model-free machine learning techniques, this approach may offer stability, practicality and efficiency advantages, especially in the area of process control [26].

This work addresses the problem of controlling discrete-time nonlinear systems with parametric uncertainties. We propose a systematic approach to obtaining a novel contraction-based controller that embeds a neural network. Firstly, we have extended continuous-time contraction analysis to the discrete-time setting, utilizing characteristics of Riemannian energy and geodesic paths at discrete time steps, and developed the corresponding discrete-time control contraction metric (DCCM) based controller design. Secondly, we have developed a novel approach that uses neural networks to synthesize DCCMs. This approach utilizes the nonlinear process model to generate two-step state trajectories, to train neural network representations of the DCCM and feedback control gain. To train the neural network, a Siamese (or twin) neural network [27], [28] is employed to ensure both steps in the state trajectory share the same state-dependent DCCM. The loss function used to train this Siamese neural network reflects the contraction conditions. Finally, conditions to ensure offset-free tracking (when system parameters are known exactly), or bounded tracking (when parameters are modeled with known uncertainty bounds), to feasible references are derived. The resulting contraction-based controller embeds a neural network.

Inspired by [26], this proposed approach trains a neural network to obtain specific contraction-based properties and a controller using a process model, integrating the power of well-studied, model-based modern control methods with the inherent ability of neural networks to handle system uncertainties. Moreover, this work provides: (1) a systematic and efficient approach to embedding neural networks in the closed-loop control scheme, and (2) certificates for stabilizability to time varying references; by imposing a contraction-based controller structure and conditions.

This article is structured as follows. Section II presents the proposed discrete-time contraction analysis and control. Section III presents the main approach to designing a discrete-time contraction-based controller for discrete-time systems with parametric uncertainties using neural networks. Section IV develops the conditions for the existence of contracting regions under the proposed neural network-based method of

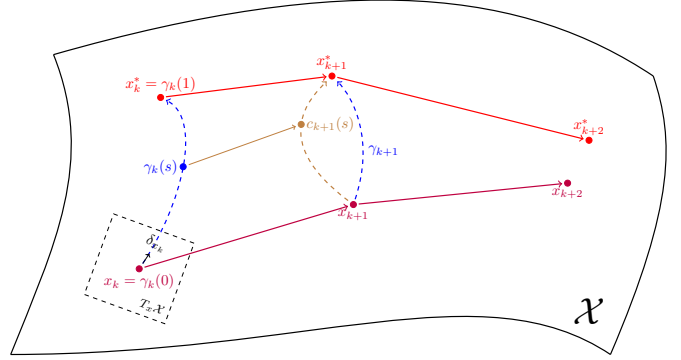


Fig. 1: Illustration of the differential dynamics of a discrete-time system along the state manifold \mathcal{X} .

Section III. Section V presents illustrative examples, followed by the conclusion Section VI concludes the article.

Notation. Function f_k is defined as $f_k = f(x_k)$ for any function f , \mathbb{Z} represents the set of all integers, \mathbb{Z}^+ represents the set of positive integers, \mathbb{R} represents set of real numbers.

II. DISCRETE-TIME CONTRACTION ANALYSIS

In this section, we complete an explicit proof for incremental exponential convergence analysis of contracting discrete-time nonlinear systems, and a controller structure for discrete-time contraction is developed (as an extension to existing continuous-time results). Conditions for discrete-time contraction-based control are then extended to handle parametric uncertainties.

To develop control approaches which are capable of delivering time-varying setpoints or reference profiles, we require reference-independent stability conditions, i.e., incremental stability (see, e.g., [29]). Contraction theory [5], [6], uses the concept of displacement dynamics or *differential dynamics* to assess incremental stability. Consider a discrete-time nonlinear system of the form,

$$x_{k+1} = f(x_k), \quad (1)$$

where $x_k \in \mathcal{X} \subseteq \mathbb{R}^n$ is state vector at time instant k , \mathcal{X} represents “restricted” state space of x_k for all k and f is a smooth differentiable function.

Define the state trajectories of (1) as $\hat{x} = (x_0, \dots, x_k, \dots)$ for $k = 0, \dots, \infty$. The group of state trajectories can be parameterized by s and thus described as $\hat{x}(s) = (x_1(s), x_2(s), \dots, x_k(s), \dots)$, where $0 \leq s \leq 1$. For example, consider the trajectory \hat{x} , associated with $s = 0$, and \hat{x}^* , associated with $s = 1$, as shown in Fig. 1. Then, consider two neighboring discrete-time trajectories separated by an infinitesimal displacement δ_{x_k} . Formally, $\delta_{x_k} := \frac{\partial x_k}{\partial s}$ is a vector in the tangent space $T_x \mathcal{X}$ at x_k . In this paper, the state manifold \mathcal{X} and the tangent space $T_x \mathcal{X}$ can both be identified with \mathbb{R}^n . The differential dynamics (or displacement dynamics) for system (1) are defined as

$$\delta_{x_{k+1}} = A_k \delta_{x_k}, \quad (2)$$

where $A_k := \frac{\partial f(x_k)}{\partial x_k}$ represents the Jacobian matrix of function f . In the context of Riemannian geometry [30], a generalized infinitesimal displacement, δ_{z_k} , can be defined using a coordinate transformation described by a mapping from δ_{x_k} to δ_{z_k} , using a square state-dependent matrix function Θ , i.e.,

$$\delta_{z_k} = \Theta(x_k)\delta_{x_k}. \quad (3)$$

If we consider the evolution of the infinitesimal squared distance for system (2) at time step k as $\delta_{x_k}^\top \delta_{x_k}$; then, naturally, the generalized squared distance for (2) can be defined using (3) as

$$\begin{aligned} V(x_k, \delta_{x_k}) &= \delta_{z_k}^\top \delta_{z_k} \\ &= \delta_{x_k}^\top \Theta(x_k)^\top \Theta(x_k) \delta_{x_k} \\ &=: \delta_{x_k}^\top M(x_k) \delta_{x_k}, \end{aligned} \quad (4)$$

where the *metric* $M(x_k) := \Theta(x_k)^\top \Theta(x_k)$ is a symmetric positive-definite matrix function and is uniformly bounded, i.e.,

$$\alpha_1 I \leq M(x_k) \leq \alpha_2 I \quad \forall x_k \in \mathcal{X}, \quad (5)$$

for some positive constants $\alpha_2 \geq \alpha_1 > 0$. We then have the following definition for a contracting system:

Definition 1 ([5]). *System (1) is contracting, with respect to a uniformly bounded metric, denoted by $M_k = M(x_k)$ and $M_{k+1} = M(x_{k+1})$, provided, $\forall x \in \mathcal{X}$ and $\forall \delta_x \in T_x \mathcal{X}$,*

$$\delta_{x_k}^\top (A_k^\top M_{k+1} A_k - M_k) \delta_{x_k} \leq -\beta \delta_{x_k}^\top M_k \delta_{x_k} < 0, \quad (6)$$

for some constant $0 < \beta \leq 1$, where (6) describes the region of contraction. In addition, the function V_k in (4) can be understood as a discrete-time Lyapunov function for the differential dynamics (2), i.e.,

$$V_{k+1} - V_k \leq -\beta V_k < 0, \quad \forall x \in \mathcal{X}, \forall \delta_x \in T_x \mathcal{X}. \quad (7)$$

The contraction region defined in (7) provides a generalized convergence condition for the discrete-time nonlinear system (1), with respect to the metric M_k . Then, following some additional definitions from Riemannian geometry, incremental stability can be established.

For a smooth curve function, $c(s) : [0, 1] \rightarrow \mathcal{X}$ (see, Fig. 1), connecting any pair of points, $x, x^* \in \mathcal{X}$ (such that $c(0) = x$ and $c(1) = x^*$), we define the Riemannian distance, $d(x, x^*)$, and energy, $E(x, x^*)$, as (see, e.g., [30])

$$\begin{aligned} d(x, x^*) &= d(c) := \int_0^1 \sqrt{\delta_{c(s)}^\top M(c(s)) \delta_{c(s)}} ds, \\ E(x, x^*) &= E(c) := \int_0^1 \delta_{c(s)}^\top M(c(s)) \delta_{c(s)} ds, \end{aligned} \quad (8)$$

where $\delta_{c(s)} := \frac{\partial c(s)}{\partial s}$. The shortest path in Riemannian space, or *geodesic*, between x_0 and x_1 is defined as

$$\gamma(s) := \arg \min_{c(s)} d(x, x^*). \quad (9)$$

A. Discrete-time Control Contraction Metrics (DCCMs)

In the following section we extend the contraction results to the controlled system setting through the use of discrete-time control contraction metrics (DCCMs). We consider a discrete-time nonlinear system in control affine form as

$$x_{k+1} = f(x_k) + g(x_k)u_k, \quad (10)$$

where $x_k \in \mathcal{X} \subseteq \mathbb{R}^n$ and $u_k \in \mathcal{U} \subseteq \mathbb{R}^m$ are the state and control vectors, respectively, \mathcal{X} and \mathcal{U} represent the restricted state and control spaces, and, f and g are smooth functions.

We define a triplet solution sequence $(x_k^*, u_k^*, x_{k+1}^*)$ for system (10) and consider the discrete-time control input, $u_k = u_k(x_k, x_k^*, u_k^*)$. The differential dynamics for system (10) satisfy

$$\delta_{x_{k+1}} = A(x_k)\delta_{x_k} + B(x_k)\delta_{u_k}. \quad (11)$$

where $A := \frac{\partial(f(x_k)+g(x_k)u_k)}{\partial x_k}$ and $B := \frac{\partial(f(x_k)+g(x_k)u_k)}{\partial u_k}$ are Jacobian matrices of functions f and g in (10) respectively, and $\delta_{u_k} := \frac{\partial u_k}{\partial s}$ is a vector in the tangent space $T_{u_k} \mathcal{U}$ at u_k . A differential state-feedback control

$$\delta_{u_k} = K(x_k)\delta_{x_k}. \quad (12)$$

is considered, which leads to the following state-feedback law:

$$u_k = u_k^* + \int_0^1 K(\gamma(s)) \frac{\partial \gamma(s)}{\partial s} ds. \quad (13)$$

Theorem 1. *Consider a discrete-time nonlinear system (10) with differential dynamics (11) and a differential state-feedback controller (12) (implemented as a state-feedback controller (13)). The above closed-loop system is contracting, with respect to a uniformly bounded DCCM, $M(x_k)$, if*

$$(A_k + B_k K_k)^\top M_{k+1} (A_k + B_k K_k) - (1 - \beta) M_k < 0, \quad (14)$$

for some constant $0 < \beta \leq 1$. Furthermore, for any feasible reference trajectory (\hat{x}^*, \hat{u}^*) (where $\hat{x}^* = (x_0^*, \dots, x_k^*, \dots)$ and $\hat{u}^* = (u_0^*, \dots, u_k^*, \dots)$) and an initial value x_0 in the contraction region given by Definition 1, the above closed-loop system is

1) *incrementally stable, i.e.,*

$$|x_k - x_k^*| \leq (1 - \beta)^{\frac{k}{2}} R |x_0 - x_0^*|, \quad (15)$$

for some constant R , where x_k is the k -th step of the closed-loop state trajectory, and

2) *incrementally exponentially stable, i.e.,*

$$|x_k - x_k^*| \leq R e^{-\lambda k} |x_0 - x_0^*|, \quad (16)$$

for some constants R and λ .

Proof. First, consider (x_k, x_{k+1}) and (x_k^*, x_{k+1}^*) as two solution pairs of system (1). The shortest path connecting each of these solutions at time step k , denoted by the geodesic $\gamma_k(s)$ in (9), is defined with $\gamma_k(0) = x_k$ and $\gamma_k(1) = x_k^*$, and $c_{k+1}(s)$ denotes a path (not necessarily a geodesic) at the next time step, connecting $c_{k+1}(0) = x_{k+1}$ and $c_{k+1}(1) = x_{k+1}^*$. Hence, from (1), we have (see, Fig. 1) $c_{k+1}(0) = x_{k+1} =$

$f(x_k) = f(\gamma_k(0))$ and $c_{k+1}(1) = x_{k+1}^* = f(x_k^*) = f(\gamma_k(1))$, or, without loss of generality

$$c_{k+1}(s) = f(\gamma_k(s)). \quad (17)$$

Then, from (8), (9) and the Hopf-Rinow Theorem, (e.g., [6]), we have

$$E(\gamma) = d(\gamma)^2 \leq d(c)^2 \leq E(c), \quad (18)$$

which, given (6) and (17), yields decreasing Riemannian energy, i.e.,

$$\begin{aligned} E(\gamma_{k+1}) &\leq \int_0^1 \frac{\partial c_{k+1}(s)}{\partial s}^\top M(c_{k+1}(s)) \frac{\partial c_{k+1}(s)}{\partial s} ds \\ &\leq \int_0^1 (1-\beta) \frac{\partial \gamma_k(s)}{\partial s}^\top M(\gamma_k(s)) \frac{\partial \gamma_k(s)}{\partial s} ds \\ &= (1-\beta)E(\gamma_k). \end{aligned} \quad (19)$$

Taking the square root of (19) gives

$$d(\gamma_{k+1}) \leq (1-\beta)^{\frac{1}{2}} d(\gamma_k). \quad (20)$$

Since M_k is by definition uniformly bounded (by two positive constants α_1 and α_2), then from (8) and (9), we have

$$\sqrt{\alpha_1}|x(k) - x^*(k)| \leq d(\gamma(k)), \quad d(\gamma(0)) \leq \sqrt{\alpha_2}|x(0) - x^*(0)|. \quad (21)$$

Combining (20) and (21) we have

$$|x_k - x_k^*| \leq (1-\beta)^{\frac{k}{2}} \sqrt{\frac{\alpha_2}{\alpha_1}} |x_0 - x_0^*|, \quad (22)$$

which for $R = \sqrt{\frac{\alpha_2}{\alpha_1}}$ concludes the result in (15).

Since the contraction rate, β , is by definition bounded as $0 < \beta \leq 1$, let $e^{-\lambda k \Delta t} = (1-\beta)^{\frac{k \Delta t}{2}}$ for some positive constant λ . Furthermore, we can express (20) with respect to a discrete-time interval, Δt , i.e.,

$$d(\gamma_{k \Delta t}) \leq (1-\beta)^{\frac{k \Delta t}{2}} d(\gamma_0) = e^{-\lambda k \Delta t} d(\gamma_0). \quad (23)$$

Then, provided the λ satisfying (23), e.g., for $\lambda = -\ln(1-\beta)/2$, we have the result in (16) by substituting (23) into (21).

Now, we consider the controlled system. The contraction condition in (14) is obtained by substituting the corresponding differential dynamic equation (11) and differential feedback control law (12) into the autonomous contraction condition (6). The control law in (13) can be obtained by integrating the differential controller (12) along the geodesic, with respect to metric, M_k , in (4) and the stability result is straightforward from the above proof by replacing the contraction condition (6) by (14). ■

To summarize, provided that the contraction condition (14) holds for the discrete-time nonlinear system (10), we can employ a stabilizing feedback controller (13) to ensure convergence to feasible operating targets.

B. Contraction of Discrete-time Uncertain Nonlinear Systems

Consider the following discrete-time control affine nonlinear system with parametric uncertainty (similar to [31], [32]):

$$x_{k+1} = f(r, x_k) + g(r, x_k)u_k, \quad (24)$$

where vector r represents the bounded uncertain parameters,

$$r \in \mathcal{R} = \{r \in \mathbb{R}^\ell \mid r_{i, \min} \leq r \leq r_{i, \max} \mid i = 1, \dots, \ell\}, \quad (25)$$

and functions f and g are smooth along the x direction and Lipschitz continuous along r . The corresponding differential dynamics (and hence the contraction condition) can be determined for any specific value of the parameter r , i.e.,

$$\delta_{x_{k+1}} = A(r, x_k)\delta_{x_k} + B(r, x_k)\delta_{u_k}, \quad (26)$$

where $A(r, x_k) := \frac{\partial(f(r, x_k) + g(r, x_k)u_k)}{\partial x_k}$ and $B(r, x_k) := \frac{\partial(f(r, x_k) + g(r, x_k)u_k)}{\partial u_k}$. The contraction-based control design for the above uncertain system requires finding a function pair (M, K) in (4) and (12), such that the contraction condition (14) holds for any $r \in \mathcal{R}$, i.e.,

$$\begin{aligned} (A_k(r) + B_k(r)K_k)^\top M_{k+1} (A_k(r) + B_k(r)K_k) \\ - (1-\beta)M_k < 0, \quad \forall r \in \mathcal{R}. \end{aligned} \quad (27)$$

Unlike condition (14), the uncertain contraction condition (27) cannot be easily, if at all, solved by SoS programming [12]. In the following sections, we will develop a neural network-based method for determining the function pair (M, K) that satisfies (27) for the full range of uncertainty, r , i.e., ensuring the contraction of uncertain system (24).

III. NEURAL NETWORK APPROACH TO CONTRACTION ANALYSIS AND CONTROL OF UNCERTAIN NONLINEAR SYSTEMS

In this section, a novel method of synthesizing a DCCM and corresponding differential state-feedback control gain for discrete-time nonlinear systems with parametric uncertainties is developed, by adopting a particular neural network structure together with a specialized loss function. This trained neural network is then embedded in a contraction-based structure for (state-feedback) real-time control.

The proposed methodology is as follows. Firstly, the family of models (24) is used to generate the state data and local values of the Jacobian matrices for training (with both arbitrary and specific distributions permitted). Secondly, the data set is fed into a neural network to learn the function pair (M, K) satisfying (27), using a tailored loss function. Finally, the controller is constructed using the function pair (M_{NN}, K_{NN}) (both of which are represented by the neural network) by implementing (13).

A. Model-based Data Generation

The first step in the proposed methodology is to generate data, \mathcal{D} , from a family of systems (24). In order to impose the contraction conditions (27) during training, which utilizes the generated data set, consideration as to which parameters must be included in \mathcal{D} is required. The Jacobian matrices, $A_k(r, x_k)$ and $B_k(r, x_k)$, can be explicitly calculated from

the system model (24) for specific r values (see (26)). If the distribution for the uncertain parameter is known, then r can be generated as a random variable with such a distribution to produce a more realistic data set for the uncertain model. Calculation of M_{k+1} requires the possible next-step states (i.e., given a specific state, $x_k \in \mathcal{X}$, generate all possible next-step states, $x_{k+1} \in \mathcal{X}$, for all possible inputs, $u_k \in \mathcal{U}$, using (24)). Consequently, the Jacobian matrices $A_k(r, x_k)$, $B_k(r, x_k)$ and the two-step trajectories, x_k, x_{k+1} , under specific r , are needed in the data set, \mathcal{D} . Algorithm 1 summarizes the data set generation procedure.

Algorithm 1: Data Set Generation.

```

Initialize  $r, s, x_k$  and  $u_k$  with lower bound values
for  $r \in \mathcal{R}$  do
  for  $x_k \in \mathcal{X}$  do
    for  $u_k \in \mathcal{U}$  do
      Calculate  $x_{k+1} = f(r, x_k) + g(r, x_k)u_k$ .
      Compute  $A_k, B_k$ .
      Store  $\{r, x_k, x_{k+1}, A_k, B_k\}_i$  in data set  $\mathcal{D}$ .
    end
  end
end

```

Remark 1. The data set generation process can be accelerated by paralleling Algorithm 1, i.e. to calculate $\{x_{k+1}, A_k, B_k\}$ with each $\{r, x_k, u_k\} \in \mathcal{R} \times \mathcal{X} \times \mathcal{U}$ in parallel.

Remark 2. An ideal data set would include all possible two-step-trajectories, x_k, x_{k+1} , and Jacobians, A_k, B_k , under all possible combinations of $r \in \mathcal{R}$, $x_k \in \mathcal{X}$, $u_k \in \mathcal{U}$. Naturally, numerical implementation of Algorithm 1 requires discretization of these continuous sets (see, e.g., (25)) using a sufficiently small step size (forming, e.g., a mesh of states). The mesh can be nonlinear, depending on the nonlinearity of the system dynamics. The mesh can also be chosen to be finer near the reference trajectories, i.e., to provide better accuracy when close to the desired state and corresponding control input. The condition on the mesh size to ensure contraction will be discussed in Section IV.

B. DCCM Synthesis from Data

In this work, a neural network is employed to represent the function pair (M, K) in (4) and (12). The structure of this neural network is shown in Fig. 2, whereby the inputs are the states of the system and the outputs are the numerical values of the matrices M_{NN} and K_{NN} for the corresponding states. Since the DCCM, M_{NN} , is a symmetric matrix, only the lower triangular components of M_{NN} are of interest (i.e., only the lower triangular matrix is required to fully construct M_{NN}). Consequently, the first group of neural network outputs are the components in the lower triangular matrix of M_{NN} and the second group of outputs are the components of the controller gain K_{NN} (see Fig. 2). Moreover, by exploiting the symmetric property of M_{NN} the computational complexity is significantly reduced (only requiring $n(n+1)/2$ decision variables or network outputs).

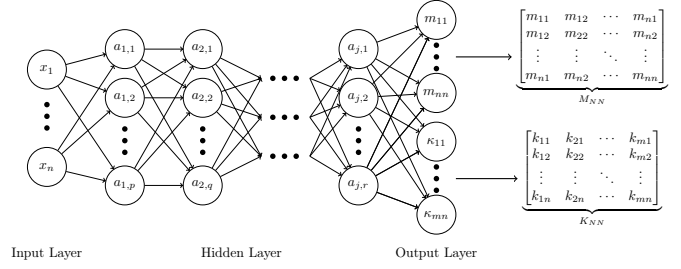


Fig. 2: Illustration of a general neural network structure.

1) *Loss Function Design:* In order to train the neural network, a suitable loss function, L , is required. Inspired by the triplet loss in [27], a novel (non-quadratic) objective loss function is developed herein to represent the positive definite properties of the neural represented metric function, M_{NN} in (4), and contraction condition (27). By reforming (27), we can rewrite the negative semi-definite uncertain contraction condition as a positive semi-definite condition (required for the subsequent loss function and training approach). Hence, we define Ω as (cf. (27))

$$\Omega := -A_{cl,k}(r)^\top M_{NN_{k+1}} A_{cl,k}(r) + (1 - \beta)M_{NN_k}, \quad (28)$$

where $A_{cl,k}(r) := A_k(r) + B_k(r)K_{NN_k}$. Then if $\Omega \geq 0$, the contraction condition (27) holds. Since these two conditions are inequalities of matrices, it is befitting to formulate the following loss function, L , based on quadratic penalty functions (see, e.g., [33])

$$L_{M_i} = \begin{cases} -(|M_{NN(1,i)}| - \epsilon_i) & \text{if } (|M_{NN(1,i)}| - \epsilon_i) \leq 0 \\ 0 & \text{else} \end{cases}$$

$$L_{\Omega_j} = \begin{cases} -(|\Omega_{(1,j)}| - \epsilon_j) & \text{if } (|\Omega_{(1,j)}| - \epsilon_j) \leq 0 \\ 0 & \text{else} \end{cases}$$

$$L = \sum_i L_{M_i} + \sum_j L_{\Omega_j}, \quad (29)$$

where $|M_{NN(1,i)}|$ is the leading principle minor of M_{NN} including the first i rows and columns (i.e square submatrix) of matrix M_{NN} and similarly for $\Omega_{(1,i)}$. Under Sylvester's criterion, by ensuring that each leading principle minor is positive, we can ensure the positive-definiteness of M_{NN} and Ω . A small positive value, ϵ_i or ϵ_j , is introduced to reduce the effects of numerical errors, which may effectively return a semi-definite (or possible non-convergence) result. Each L_{M_i} or L_{Ω_j} returns a higher cost if the leading principle minor is smaller than ϵ_i or ϵ_j , otherwise, it returns zero. This encourages convergence of the leading principle minor to some value larger than ϵ_i or ϵ_j . The loss function, L , (the sum of all L_{M_i} and L_{Ω_j}), encourages all leading principle minors to be positive and hence the positive definiteness of both matrices, M_{NN} and Ω , which consequently implies M_{NN} is a DCCM for the contraction of (24). Compared to existing CCM synthesis approaches using SoS programming, the proposed method permits contraction metric and feedback gain synthesis for non-polynomial system descriptions in addition to systems modeled with parametric uncertainty.

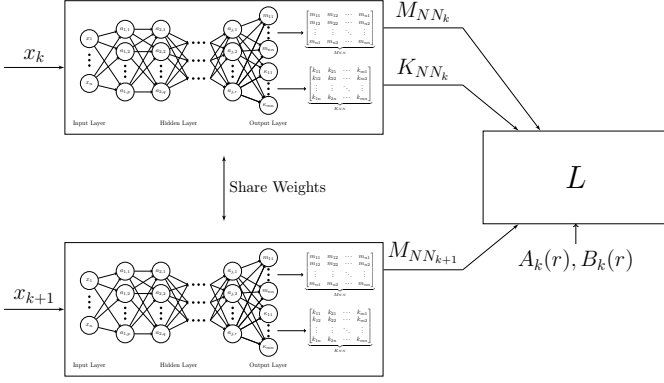


Fig. 3: Training process block diagram.

2) *Neural Network Training*: Using the training data set, \mathcal{D} , generated from Algorithm 1 and loss function (29), we detail here the process for training the neural network function pair (M_{NN}, K_{NN}) . The neural network cannot be simply trained using the generalized structure in Fig. 2, as the loss function (29) requires both the neural network output under input, x_k , and also the output under input, x_{k+1} , since (28) requires both M_{NN_k} and $M_{NN_{k+1}}$ at the next step (i.e., $M_{NN}(x_{k+1})$ evaluated using $M_{NN}(x_k)$ and stepping forward using (24)). To overcome this difficulty, we adopted a Siamese network (see Fig. 3) structure, whereby two neural networks, sharing the same weights, can be tuned at the same time, by considering both outputs of the weight sharing neural networks simultaneously. In addition, the Siamese network structure permits the use of outputs at time step k and $k+1$ in the loss function. Furthermore, the learning can be done in parallel using a GPU to speed up the training, i.e. the complete set, \mathcal{D} is treated as a batch, and a total loss, L_t , is defined by summing every loss function, L_i , where L_i is the output from each element $\{r, x_k, x_{k+1}, A_k, B_k\}_i$ in \mathcal{D} . Algorithm 2 describes the training procedure for the Siamese neural network, with further details and discussion provided subsequently.

Algorithm 2: Training Procedure

Stack elements, $\{r, x_k, x_{k+1}, A_k, B_k\}_i \in \mathcal{D}$ as a batch
for $iter \leq \text{max iteration number}$ **do**
 for *each element* $\{r, x_k, x_{k+1}, A_k, B_k\}_i \in \mathcal{D}$ **do**
 Feed x_k into the Siamese neural network.
 Feed x_{k+1} into the Siamese neural network.
 Construct $M_{NN_k}, M_{NN_{k+1}}$ and K_{NN_k} .
 Calculate the i -th element loss, L_i , as in (29).
 end
 Calculate total loss $L_t = \sum_i L_i$.
 Proceed backward propagation.
 if $L_t < \epsilon_{min}$ **then**
 | Break.
 end
end
Save M_{NN} and K_{NN} .

The first step in Algorithm 2, is to feed the two-step trajectories, x_k, x_{k+1} , into the Siamese networks, which have two sets

of outputs, M_{NN_k}, K_{NN_k} and $M_{NN_{k+1}}$. Then, M_{NN_k}, K_{NN_k} and $M_{NN_{k+1}}$ are used to calculate the loss function, L_i (29) for $\{r, x_k, x_{k+1}, A_k, B_k\}_i$. The neural network is trained using backward propagation, whereby the loss is summed cumulatively at each iteration. As described in Algorithm 2, each iteration involves calculating the total loss, L_t , for the all elements in the data set; however, if the number of elements is sufficiently large, this process can be batch executed. The learning process is finally terminated when the total loss, L_t , is small enough, or the max number of predefined iterations is reached. The error threshold, ϵ_{min} , is the smallest among all ϵ_i or ϵ_j in (29), which implies that provided the cumulative error is lower than this threshold, the contraction condition is satisfied for each point in the data set.

Remark 3. A number of existing strategies are available for quantifying the “success” of a trained neural network, e.g., through testing and verification (see, e.g., [34]–[36]) or statistical analysis and performance metrics (see, e.g., [37], [38]). As an example, we note that the training methodology presented, is capable of incorporating direct validation by splitting or generating multiple data sets, say one for training, \mathcal{D}_T , and another for validation, \mathcal{D}_V , whereby each set can be given context specific weighting, pending, e.g., the target system trajectories or known regions of typical or safety critical operation. Due to the task specific nature of this process and range of techniques available, we have omitted its presentation here for clarity and refer the interested reader to [34], [39], [40] for further details. Herein, and without loss of generality, we assume the training process was completed sufficiently, i.e., the training process was not stopped due to exceeding the maximum number of iterations, with a level of accuracy sufficient for the desired control application.

C. Neural Network Embedded Contraction-based Controller

This section details the implementation of a contraction-based controller, of the form in (13), that is obtained by embedding a neural network representation of the function pair (M, K) , i.e., M_{NN} and K_{NN} (calculated using Algorithms 1 and 2). Foremost, the proposed neural network embedded contraction-based controller is described by (cf. (13))

$$u_k = u_k^* + \int_0^1 K_{NN}(\gamma(s)) \frac{\partial \gamma(s)}{\partial s} ds, \quad (30)$$

where (x_k^*, u_k^*) are the state and control reference trajectories at time k . When the desired state value, x_k^* , changes, the feed-forward component, u_k^* , can be instantly updated, and the feedback component, $\int K_{NN} \delta_\gamma ds$, can be automatically updated through online geodesic calculation. Note that this approach results in setpoint-independent control synthesis. From (8) and (9), the geodesic, γ , is calculated as

$$\begin{aligned} \gamma(x, x^*) &:= \arg \min_c d(x, x^*) \\ &= \arg \min_c \int_0^1 \frac{\partial c(s)}{\partial s}^T M_{NN}(c(s)) \frac{\partial c(s)}{\partial s} ds, \end{aligned} \quad (31)$$

where M_{NN} and K_{NN} are the function pair (M, K) represented by the neural network (see Fig. 2), and recall from

Section II-A that $c(s)$ is an s -parameterized smooth curve connecting x ($s = 0$) to x^* ($s = 1$). Implementing the contraction-based controller (13) requires integrating the feedback law along the geodesic, γ , in (9). Subsequently, one method to numerically approximate the geodesic is shown. Since (31) is an infinite dimensional problem over all smooth curves, without explicit analytical solution, the problem must be discretized to be numerically solved. Note that the integral can be approximated by discrete summation provided the discrete steps are sufficiently small. As a result, the geodesic (31) can be numerically calculated by solving the following optimization problem,

$$\begin{aligned} \bar{\gamma}(x, x^*) = \arg \min_{\Delta x_s} \sum_{i=1}^N \Delta x_{s_i}^T M_{NN}(x_i) \Delta x_{s_i} \Delta s_i \\ \text{s.t. } x_1 = x, x_N = x^*, \end{aligned} \quad (32)$$

where $\bar{\gamma}(x, x^*) \approx \gamma(x, x^*)$ represents the numerically approximated geodesic, x and x^* are the endpoints of the geodesic, $\Delta x_{s_i} := \Delta x_i / \Delta s_i \approx \partial c(s) / \partial s$ can be interpreted as the displacement vector discretized with respect to the s parameter, $\Delta x_s := (\Delta x_{s_1}, \dots, \Delta x_{s_N})$ is the discretized path joining x to x^* (i.e., discretization of $c(s)$ in (31)), all Δs_i are small positive scalar values chosen such that $\sum_{i=1}^N \Delta s_i = 1$, N is the chosen number of discretization steps (of s), $x_i = \sum_{j=1}^i \Delta x_{s_j} \Delta s_j + x$ represents the numerical state evaluation along the geodesic.

Remark 4. Note that (32) is the discretization of (31) with Δx_{s_i} and Δs_i as the discretizations of $\frac{\partial c(s)}{\partial s}$ and δ_s respectively. Furthermore, note that the constraints in (32) ensure that the discretized path connecting the start, x , and end, x^* , state values align with the continuous integral from $s = 0$ to $s = 1$. Hence, as Δs_i approaches 0, i.e., for an infinitesimally small discretization step size, the approximated discrete summation in (32) converges to the smooth integral in (31).

After the geodesic is numerically calculated using (32), the control law in (13) can be analogously calculated using an equivalent discretization as follows

$$u_k = u_k^* + \sum_{i=1}^N \Delta x_{s_i} \Delta s_i K_{NN}(x_i). \quad (33)$$

The state reference, x^* , is chosen to follow some desired trajectory, for which the corresponding instantaneous input, u^* , can be computed via real-time optimization methods (see ‘‘Reference Generator’’ in Fig. 4), such that the triplet $(x_k^*, u_k^*, x_{k+1}^*)$ satisfies (24), i.e.,

$$x_{k+1}^* = f(r^*, x_k^*) + g(r^*, x_k^*) u_k^*, \quad (34)$$

for a specific value of the uncertain parameter, $r = r^*$. The choice for this specific value, for the purpose of reference design, can be selected as the most likely or expected value for the uncertain parameter, i.e., $\bar{r} := \mathbb{E}[r]$. Hence, the corresponding desired control input at any time, u_k^* , can be calculated from (24) as the expected corresponding control effort, $\bar{u}_k := \mathbb{E}[u_k^*]$, given both the desired state values,

x_k^*, x_{k+1}^* , and expected parameter, $r = \bar{r}$. Suppose then, that there was some error (e.g., due to modeling) between the chosen uncertain parameter, r^* , and the exact value for r . Consequently, there will be some error when computing the corresponding control effort for the desired state trajectory (via (24)), and moreover, for the resulting control effort in (30), denoted by $\tilde{u}_k = \bar{u}_k - u_k^*$. The resulting *disturbed* system, can be modeled, using (24), as

$$x_{k+1} = f(r, x_k) + g(r, x_k)(u_k + \tilde{u}_k), \quad (35)$$

where u_k has the same form as (13). Inspired by the results in [5], we have then have the following contraction result.

Lemma 1. For the disturbed system (35), with contraction-based controller (13), the state trajectory, x , converges to a bounding ball around the target reference, x^* , described by

$$d(\gamma_{k+1}) - (1 - \beta)^{\frac{1}{2}} d(\gamma_k) \leq \sqrt{\alpha_2} G_k \|\tilde{u}_k\|. \quad (36)$$

Proof. A Riemannian space is a metric space, thus from the definition of a metric function (see e.g., [41]) we have the following inequality,

$$\begin{aligned} d(\gamma(x_{k+1}, x_{k+1}^*)) &= d(\gamma(\tilde{x} + g(r, x_k) \tilde{u}_k, x_{k+1}^*)) \\ &\leq d(\gamma(\tilde{x}_{k+1}, x_{k+1}^*)) + d(\gamma(\tilde{x}_{k+1} + g(r, x_k) \tilde{u}_k, \tilde{x}_{k+1})), \end{aligned} \quad (37)$$

where $\tilde{x}_{k+1} := f(r, x_k) + g(r, x_k) u_k$. Now, we consider the last two components of (37). Firstly, from (20), we have $d(\gamma(\tilde{x}_{k+1}, x_{k+1}^*)) \leq (1 - \beta)^{\frac{1}{2}} d(\gamma(x_k, x_k^*))$. Secondly, since the metric, M_k , is bounded (5), then, $d(\gamma(\tilde{x}_{k+1} + g(r, x_k) \tilde{u}_k, \tilde{x}_{k+1})) \leq \sqrt{\alpha_2} G_k \|\tilde{u}_k\|$, where $G_k = \max_{x_k} \|g(r, x_k)\|$. Thus we have the conclusion in (36). ■

Remark 5. The condition in (36) requires the disturbance term, $g_k \tilde{u}_k$ in (35), to be bounded. The control deviation, \tilde{u}_k is a constant, given a particular value for r , and it is a reasonable assumption that in control practice, the control-to-state mapping, g_k , is also bounded for all k .

The choice for the uncertain parameter, r^* , when designing the reference trajectory, (x^*, u^*) , directly affects the radius of the ball to which the system (10) contracts, and naturally, a finite upper limit on the radius, due to this design choice, exists and can be described by the maximum disturbance, i.e., $\max \sqrt{\alpha_2} \|g_k \tilde{u}_k\|$. For continuity, note that by designing the reference about the expected value of the uncertain parameter, i.e., $r^* = \bar{r}$, the expected radius of the bounding ball in (36) is zero and hence (cf. (20)) recovers the undisturbed or exact contraction results of Section II.

The proposed contraction-based controller embeds a neural network, as shown in Fig. 4. At each step, the state measurement, x_k , is fed into the neural network to determine the metric and feedback gain, M_{NN} and K_{NN} . The numerical geodesic, Δx_s , and control input reference, u^* , are determined using two separate real-time optimization modules. The control action, u_k is then calculated using (33) based on the geodesic and control input reference.

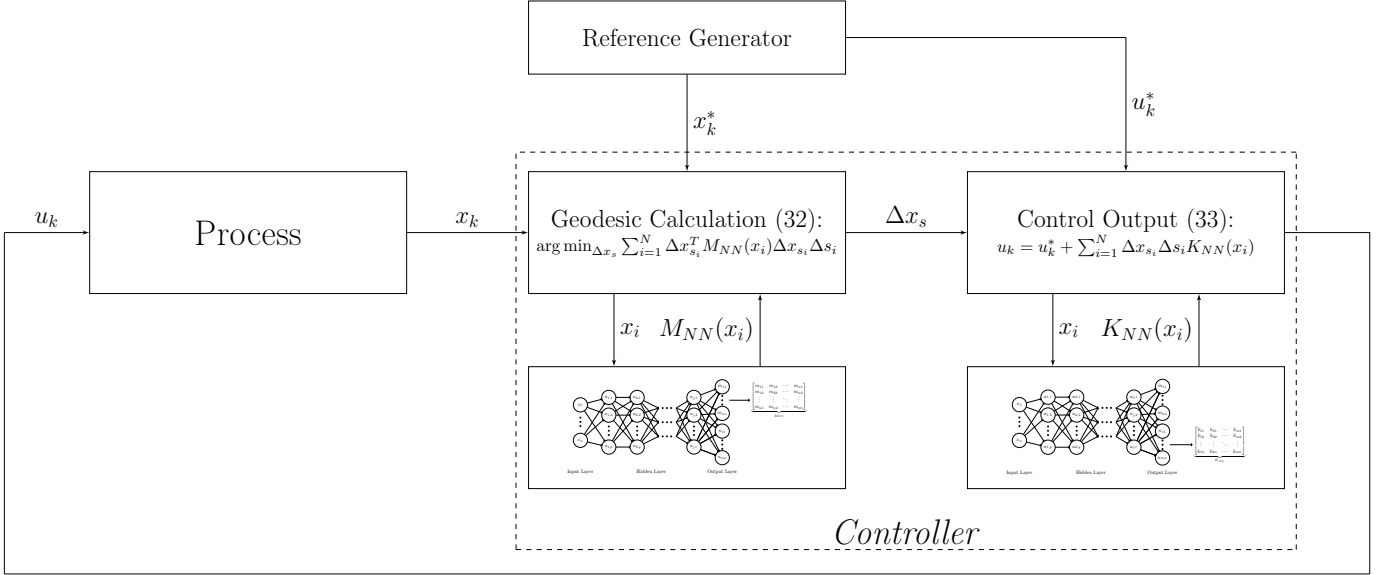


Fig. 4: Proposed neural network embedded contraction-based control scheme.

IV. DESIGN ANALYSIS

In practice, the neural network should be trained with a finite data set to make. Using Algorithms 1 and 2, the finite data set \mathcal{D} is comprised of a grid of points in \mathcal{R} , \mathcal{X} , \mathcal{U} , which naturally depends on the discretization step size or grid resolution (see Remark 2). In this section we develop bounding conditions on the contraction properties for the entire region of interest, when only a discrete number of data points are available. For clarity of presentation, we begin with considering the control affine system without uncertainty in (10). The following theorem describes contraction regions in the form of a finite ball surrounding a known contracting point.

Theorem 2. *If the contraction condition in (14) holds for a state and control value pair (x^*, u^*) (satisfying (10)), then there exists a ball $B((x^*, u^*), \xi)$ with radius $\xi = (\xi_x, \xi_u)$, centered at (x^*, u^*) , in which the system (10) is locally contracting with a rate no slower than $\lambda - L_{xu}\|\xi\|$, where λ is the desired contraction rate and L_{xu} is a Lipschitz constant.*

Proof. Consider a function

$$h(x_k, u_k) := \max \text{eig}((\Theta_k^{-1})^\top A_{cl,k}^\top M_{k+1} A_{cl,k} \Theta_k^{-1} - I), \quad (38)$$

where $A_{cl,k} := A_k + B_k K_k$. Since all arguments of h are assumed to be smooth, we can apply a Lipschitz condition to function h , yielding

$$|h(x^* + \xi_x, u^* + \xi_u) - h(x^*, u^*)| \leq L_{xu} \|\xi\|, \quad (39)$$

where L_{xu} is a Lipschitz constant. By definition [5], we have $h(x_k, u_k) \leq -\lambda$. Hence, the largest variation of h inside the ball can be upper bounded by

$$h(x^* + \xi_x, u^* + \xi_u) \leq h(x^*, u^*) + L_{xu} \|\xi\| \leq -\lambda + L_{xu} \|\xi\|. \quad (40)$$

Provided $-\lambda + L_{xu} \|\xi\| < 0$, the system (10) is contracting inside the ball, for which, there always exists a $\|\xi\|$ to ensure this negative condition. Moreover, the minimum contraction

rate can be directly obtained by considering the maximum eigenvalue inside the ball. ■

Theorem 2 describes a local contraction property in the space $\mathcal{X} \times \mathcal{U}$. This property is generalized to the space \mathcal{X} in the following extension, by considering all possible control values, $u \in \mathcal{U}$, for a particular state value, $x^* \in \mathcal{X}$.

Corollary 1. *If the ball $B((x^*, u^j), \xi)$ centered at (x^*, u^j) forms a local contraction region for the system in (10) (for some control value u^j), and $B_x(x^*, \xi_x) \times \mathcal{U} \subseteq \bigcup_j B((x^*, u^j), \xi)$, then the system is locally contracting within $\bigcup_j B_x(x^*, \xi_x)$ at x^* .*

Proof. From (38), we have the contraction condition holds at different u^j with radius ξ_u . If these balls are connected, then, there exists a ball around x^* such that $B_x(x^*, \xi_x) \times \mathcal{U} \subseteq \bigcup_j B((x^*, u^j), \xi)$. ■

These results are extended in the following to systems with parametric uncertainties by considering locally contracting regions in the space $\mathcal{X} \times \mathcal{U} \times \mathcal{R}$ and hence the entire space of uncertainty, \mathcal{R} .

Corollary 2. *If the contraction condition in (27) holds for the uncertain parameter value r^* with state and control pair (x^*, u^*) for the system (24), then there exists a ball $B((x^*, u^*, r^*), \xi)$ with radius $\xi = (\xi_x, \xi_u, \xi_r)$ centered at (x^*, u^*, r^*) , for which the system (24) is locally contracting. Moreover, if $B_x(x^*, \xi_x) \times \mathcal{U} \times \mathcal{R} \subseteq \bigcup_{j,\ell} B((x^*, u^j, r^\ell), \xi)$, the system is locally contracting within $B_x(x^*, \xi_x)$ at x^* .*

Proof. These results are straightforward extensions of Theorem 2 and Corollary 1, by considering an additional parameter r and hence dimension, i.e., $\forall r \in \mathcal{R}$. ■

By combining multiple locally contracting regions, a larger region of interest, \mathcal{S} , can be formed, for which we have the following immediate result.

Corollary 3. *If there exist multiple locally contracting regions $B_{x,i} := B_x(x^i, \xi_{x,i})$ such that $S_x \subseteq \bigcup_i B_{x,i}$ (where $S_x \subseteq \mathcal{X}$ is an area of interest), then the area S_x^i is a contraction region with the minimum contraction rate $\lambda_{S_x, \min}$ given by*

$$\lambda_{S_x, \min} = \min_i (\lambda - L_{xur} \|\xi_i\|). \quad (41)$$

Proof. This result is straightforward from Theorem 2, by following a similar approach to the proof of Corollary 1, where $h(x^* + \xi_x, u^* + \xi_u, r^* + \xi_r) \leq -\lambda + L_{xur} \|\xi\|$ and L_{xur} is a Lipschitz constant. The minimum contraction rate inside the region of interest is obtained by considering the maximum eigenvalue among local contraction regions covering the whole space of interest S_x . ■

Theorem 2 and Corollaries 1–3 state that the contraction property of a nonlinear system with parametric uncertainty can be determined by checking a finite number of local conditions (e.g., across a grid of state values). In this way, a contraction rate close to the desired one can be achieved for an uncertain nonlinear system (10) using finite data sets, hence making Algorithms 1 and 2 tractable. As the number of data points increases (and hence, considering increasingly small balls about each point), the minimum contraction rate for the unified region of interest, S_x , approaches the desired contraction rate. Likewise, as the number of data points is reduced, the guaranteed contraction rate deviates further from the desired rate. As such, the proposed controller can be used to control systems with or without parametric uncertainties.

V. ILLUSTRATIVE EXAMPLES

Several simulation studies are presented in this section to illustrate the proposed control design method and control performance for both certain and uncertain nonlinear discrete-time systems. The following simulations use PyTorch [42] and SciPy [43] with an Intel i9700k CPU, 16GB RAM and an Nvidia 2080Ti GPU.

A. Discrete-time Lotka-Volterra System without Uncertainty

Consider the following Euler discretized Lotka–Volterra model which describes a predator–prey ecosystem [44]:

$$\begin{bmatrix} x_{1_{k+1}} \\ x_{2_{k+1}} \end{bmatrix} = \begin{bmatrix} 1.1x_{1_k} - 0.1x_{1_k}x_{2_k} + u_k \\ 0.9x_{2_k} + 0.1x_{1_k}x_{2_k} \end{bmatrix}, \quad (42)$$

where x_1 denotes the number of prey, x_2 is the number of predators and u is the human interaction, including prey removal ($u < 0$) and introduction of prey into the ecosystem ($u > 0$). The state and input constraints are $x_{1_k} \in [0.5, 1.5]$, $x_{2_k} \in [0.5, 1.5]$ and $u_k \in [-1, 1]$.

We illustrate the training of the neural network for the function pair (M_{NN}, K_{NN}) (see Fig. 2) that satisfies the contraction condition in (14). Firstly, the data used to train the neural network are collected as per Algorithm 1. Using a square mesh of state x_k and control u_k (with the steps of 0.02

and 0.1, respectively), the data spanning the state and control constrained space are generated. This is used to compute the corresponding next time step state values, x_{k+1} , resulting in the set $\{x_k, x_{k+1}\}_i$. The Jacobian matrix is also calculated for each state point on the mesh, i.e.

$$A_k = \begin{bmatrix} 1.1 - 0.1x_{2_k} & -0.1x_{1_k} \\ 0.1x_{1_k} & 0.9 + 0.1x_{1_k} \end{bmatrix}, B_k = \begin{bmatrix} 1 \\ 0 \end{bmatrix}. \quad (43)$$

The Jacobians are then appended, to obtain the component $\{x_k, x_{k+1}, A_k, B_k\}_i$, where i numbers each combination of state and control input and we can ignore the set of elements if x_{k+1} is outside the constraints. The collection of each i -th component forms the training data set, \mathcal{D} .

TABLE I: Neural Network Training Parameters.

Parameters	Value
β_1	0.1
β_2	0.9
Learning rate	0.05
Weight decay coefficient	0.5
Hidden layer number	3
Each hidden layer neurons	15
Hidden layer activation	ReLU
Input layer activation	Linear
Output layer activation	Linear

Secondly, the neural network is constructed as in Fig. 3 and Fig. 2 using the AdamW [45] algorithm with default settings and the parameters listed in Table I. The outputs of the neural network form the DCCM, M_{NN} , and differential controller gain, K_{NN} , which is defined in following equation,

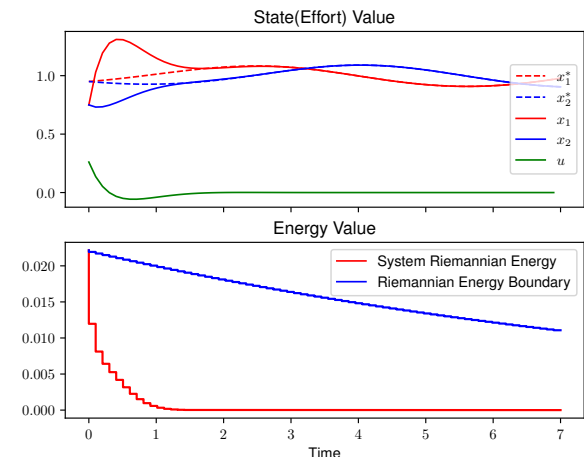
$$M_{NN} = \begin{bmatrix} m_1 & m_2 \\ m_2 & m_3 \end{bmatrix}, K_{NN} = \begin{bmatrix} \kappa_1 \\ \kappa_2 \end{bmatrix}. \quad (44)$$

The data set, \mathcal{D} , is fed into the neural network to minimize the loss function using Algorithm 2. The neural network represented function pair (M_{NN}, K_{NN}) can be obtained as per Section IV (i.e., Theorem 2 and Corollary 1–3).

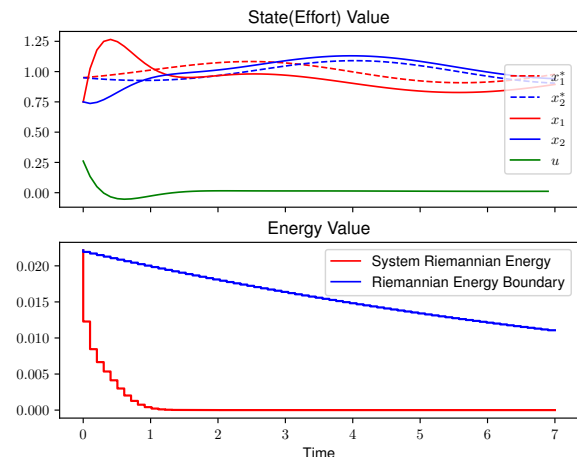
Finally, using (M_{NN}, K_{NN}) , the controller (30) is implemented to track the time varying reference, x^* , and corresponding input reference, u^* , satisfying

$$\begin{bmatrix} x_{1_{k+1}}^* \\ x_{2_{k+1}}^* \end{bmatrix} = \begin{bmatrix} 1.1x_{1_k}^* - 0.1x_{1_k}^*x_{2_k}^* \\ 0.9x_{2_k}^* + 0.1x_{1_k}^*x_{2_k}^* \end{bmatrix}, \quad u^* = 0, \quad (45)$$

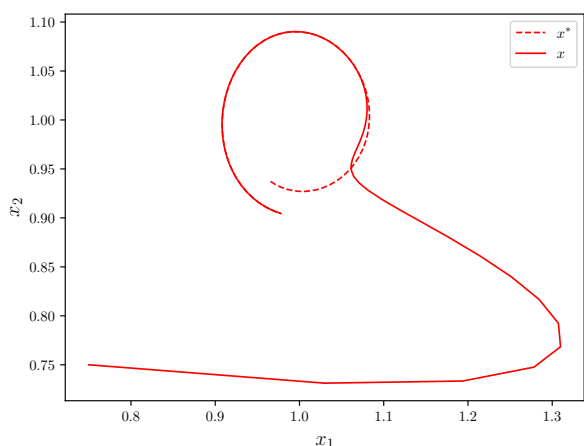
with initial condition $(x_{1_{ini}}^*, x_{2_{ini}}^*) = (0.85, 0.85)$. Note that (45) describes stable orbits (since the input is zero), each dependent on the initialization. The initial condition for the system is chosen to be $(x_{1_{ini}}, x_{2_{ini}}) = (0.65, 0.65)$ and hence control effort, $u \neq 0$, will be required to drive the system to the desired stable orbit, i.e., in order to achieve the desired stable ecosystem without human involvement, $u = 0$, some human involvement will be required. The simulation results are presented in Fig. 5. Observe that the system converges to the state and control references and that the Riemannian energy is both decreasing and bounded as per Theorem 1.



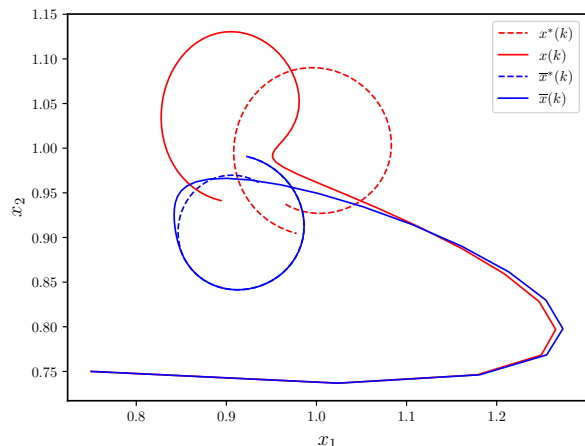
(a) System response and Riemannian energy.



(a) System response and Riemannian energy.



(b) Phase plot.



(b) Phase plot comparison.

Fig. 5: Simulation without uncertainty.

Fig. 6: Simulation with uncertain parameter $r = 1.1$.

B. Discrete-time Lotka-Volterra System with Uncertainty

To illustrate the ability of the proposed control approach to handle parametric uncertainties, consider the system in (42) with an uncertain parameter r :

$$\begin{bmatrix} x_{1k+1} \\ x_{2k+1} \end{bmatrix} = \begin{bmatrix} 1.1x_{1k} - 0.1rx_{1k}x_{2k} + u_k \\ 0.9x_{2k} + 0.1rx_{1k}x_{2k} \end{bmatrix}, \quad (46)$$

where the state and input constraints are $x_{1k} \in [0.5, 1.5]$, $x_{2k} \in [0.6, 1.4]$ and $u_k \in [-1, 1]$. The uncertain parameter $r \in [0.9, 1.1]$ with the true value of $r = 1$, represents how often the two species, x_1 and x_2 , meet due to environmental conditions.

The data to be used for training can be generated using r of different values with steps of 0.1 and executing the same process of Section V-A to compute $\{r, x_k, x_{k+1}, A_k, B_k\}_i$ and \mathcal{D} , with the parameters in Table I. The target time-varying reference, (x^*, u^*) , satisfying (45), is calculated as in Section V-A using $r = 1$ and initial condition $(x_{1ini}^*, x_{2ini}^*) = (1.1, 1.1)$. Simulations were carried out, using the same neural network-based controller without retraining for $r = 1.1$, with

the initial condition of the system set to $(x_{1ini}, x_{2ini}) = (0.75, 0.75)$. The results shown in Fig. 6 demonstrate that the neural network-based contraction controller (30) was capable of tracking a time-varying reference (achieving a stable ecosystem free from human involvement) within a bounded distance (close to the desired orbit, as per Lemma 1), despite not knowing the exact value of r , without the need for controller redesign or adjustment. As discussed in Section III-C, an offset occurs because the reference generator could not provide a correct reference orbit or the control reference u^* due to the uncertain parameter (from the perspective of the reference model, relative to the actual value). Fig. 6a shows that the Riemannian energy is decreasing and bounded as per Lemma 1 (considering (8) and (36), i.e., the bounded Riemannian energy as the bounded squared length). Fig. 6b also shows that the system (\bar{x}) tracks the reference without error if when r in the model has a true value.

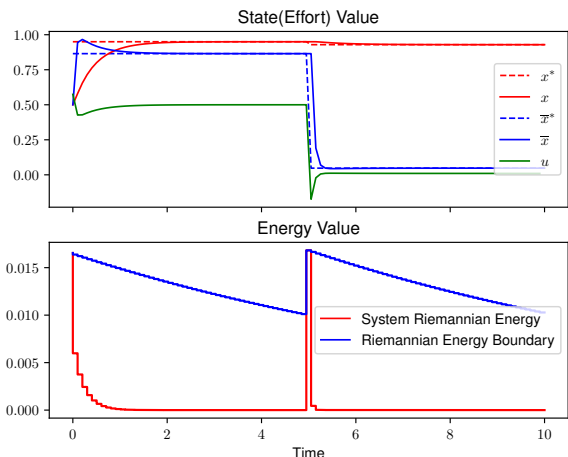


Fig. 7: Simulation of a CSTR without uncertainty.

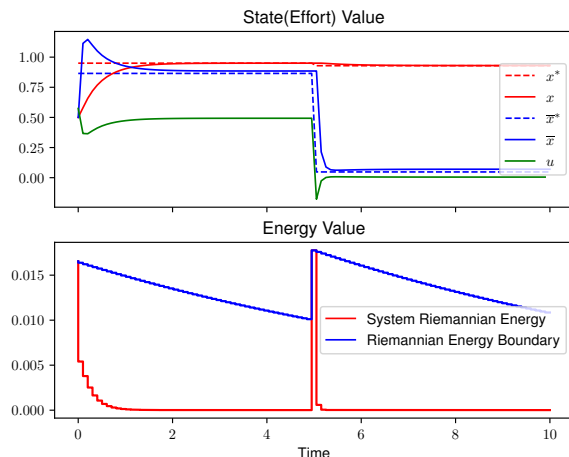


Fig. 8: Simulation of a CSTR with uncertainty.

C. Discrete-time CSTR

Consider the following Euler discretized nonlinear CSTR model [4] which has more complex nonlinear dynamics:

$$\begin{bmatrix} x_{1k+1} \\ x_{2k+1} \end{bmatrix} = \begin{bmatrix} 0.9x_{1k} + 0.1\phi_1(x_{1k})e^{\frac{\alpha x_{2k}}{\alpha+x_{2k}}} + 0.1(1-\zeta)x_{1k} \\ 0.9x_{2k} + 0.1B\phi_2(x_{1k})e^{\frac{\alpha x_{2k}}{\alpha+x_{2k}}} + u_k \end{bmatrix},$$

where $\phi_i(x_{1k}) = Da_i(1 - x_{1k})$, $Da_1 = 1.25$, $Da_2 = 2.5$, $\zeta = 0.1$, $\alpha = 0.8$ and the uncertain parameter $B \in [1, 2]$ with the true value $B = 1$. The state and input constraints are $x_{1k} \in [0.1, 1.1]$, $x_{2k} \in [0.1, 1.1]$ and $u_k \in [-1, 1]$, respectively. The normalized reactant concentration, reactor temperature and jacket temperature are denoted by x_{1k} , x_{2k} and u_k , respectively. Data generation is conducted using Algorithm 1 via a square mesh of state (x_k) and control (u_k) values, with steps of $\frac{1}{80}$ and $\frac{1}{10}$, respectively. The function pair (M_{NN}, K_{NN}) are trained using Algorithm 2 with the neural network structure and training parameters as in Sections V-B. The time-varying state and control setpoints are given as

$$(x_1^*(t), x_2^*(t), u^*(t)) = \begin{cases} (0.9499, 0.8650, 0.5), & \forall t \in [0, 5) \\ (0.9290, 0.0476, 0.01), & \forall t \in [5, 10]. \end{cases}$$

Fig. 7 shows that the discrete-time neural network embedded contraction-based controller (33) is capable of offset-free tracking, when the exact model is known. Also observe that the Riemannian energy is both decreasing and bounded. Moreover, Fig. 8 illustrates that the proposed approach achieves bounded reference tracking (as per Lemma 1) when parametric modeling uncertainty is present.

VI. CONCLUSION

In this article, a framework was developed that permits the use of a nonlinear system model, with uncertainty, to train a neural network (contraction metric and feedback gain) for contraction analysis and control. Considerations were made for the discrete-time contraction and stability for certain nonlinear systems, which for known bounds on modeling uncertainty, were then extended to provide direct analysis and controller

synthesis tools for the contraction of uncertain nonlinear systems. The resulting contraction-based controller, which embeds the trained neural network, was shown capable of achieving efficient tracking of time-varying references, for the full range of model uncertainty, without the need for controller structure redesign.

REFERENCES

- [1] C. Zhang, Z. Shao, X. Chen, X. Gu, L. Feng, and L. T. Biegler, "Optimal flowsheet configuration of a polymerization process with embedded molecular weight distributions," *AIChE Journal*, vol. 62, no. 1, pp. 131–145, 2016.
- [2] N. N. Chokshi and D. C. McFarlane, "DRPC: Distributed reconfigurable process control," *A Distributed Coordination Approach to Reconfigurable Process Control*, pp. 43–49, 2008.
- [3] R. Wang and J. Bao, "Distributed plantwide control based on differential dissipativity," *International Journal of Robust and Nonlinear Control*, vol. 27, no. 13, pp. 2253–2274, 2017.
- [4] R. McCloy, R. Wang, and J. Bao, "Differential dissipativity based distributed MPC for flexible operation of nonlinear plantwide systems," *Journal of Process Control*, vol. 97, pp. 45–58, 2021.
- [5] W. Lohmiller and J.-J. E. Slotine, "On contraction analysis for non-linear systems," *Automatica*, vol. 34, no. 6, pp. 683–696, 1998.
- [6] I. R. Manchester and J.-J. E. Slotine, "Control contraction metrics: Convex and intrinsic criteria for nonlinear feedback design," *IEEE Transactions on Automatic Control*, vol. 62, no. 6, pp. 3046–3053, 2017.
- [7] B. T. Lopez and J. E. Slotine, "Adaptive nonlinear control with contraction metrics," *IEEE Control Systems Letters*, vol. 5, no. 1, pp. 205–210, 2021.
- [8] I. R. Manchester and J.-J. E. Slotine, "Robust control contraction metrics: A convex approach to nonlinear state-feedback H^∞ control," *IEEE Control Systems Letters*, vol. 2, no. 3, pp. 333–338, 2018.
- [9] S. Singh, A. Majumdar, J. Slotine, and M. Pavone, "Robust online motion planning via contraction theory and convex optimization," in *International Conference on Robotics and Automation (ICRA)*, 2017, pp. 5883–5890.
- [10] S. Singh, S. M. Richards, V. Sindhwani, J.-J. E. Slotine, and M. Pavone, "Learning stabilizable nonlinear dynamics with contraction-based regularization," *The International Journal of Robotics Research*, 2020.
- [11] G. C. Goodwin, S. F. Graebe, M. E. Salgado *et al.*, *Control System Design*. Upper Saddle River, NJ: Prentice Hall, 2001.
- [12] L. Wei, R. McCloy, and J. Bao, "Control contraction metric synthesis for discrete-time nonlinear systems," in *11th IFAC SYMPOSIUM on Advanced Control of Chemical Processes (accepted)*, 2021.
- [13] E. M. Aylward, P. A. Parrilo, and J.-J. E. Slotine, "Stability and robustness analysis of nonlinear systems via contraction metrics and sos programming," *Automatica*, vol. 44, no. 8, pp. 2163–2170, 2008.

- [14] S. Chen, S. Billings, and P. Grant, "Non-linear system identification using neural networks," *International Journal of Control*, vol. 51, no. 6, pp. 1191–1214, 1990.
- [15] S.-L. Dai, C. Wang, and M. Wang, "Dynamic learning from adaptive neural network control of a class of nonaffine nonlinear systems," *IEEE Transactions on Neural Networks and Learning Systems*, vol. 25, no. 1, pp. 111–123, 2013.
- [16] G. Cybenko, "Approximation by superpositions of a sigmoidal function," *Mathematics of Control, Signals and Systems*, vol. 2, no. 4, pp. 303–314, 1989.
- [17] L. Niu, "Adaptive neural network control for uncertain nonlinear systems with asymptotic stability guarantees," in *5th International Conference on Intelligent Human-Machine Systems and Cybernetics*, vol. 2, 2013, pp. 546–549.
- [18] A. Draeger, S. Engell, and H. Ranke, "Model predictive control using neural networks," *IEEE Control Systems Magazine*, vol. 15, no. 5, pp. 61–66, 1995.
- [19] T. Wang, H. Gao, and J. Qiu, "A combined adaptive neural network and nonlinear model predictive control for multirate networked industrial process control," *IEEE Transactions on Neural Networks and Learning Systems*, vol. 27, no. 2, pp. 416–425, 2015.
- [20] S. S. Ge, C. C. Hang, T. H. Lee, and T. Zhang, *Stable Adaptive Neural Network Control*. Springer Science & Business Media, 2013, vol. 13.
- [21] P. Vincent, H. Larochelle, Y. Bengio, and P.-A. Manzagol, "Extracting and composing robust features with denoising autoencoders," in *Proceedings of the 25th International Conference on Machine Learning*, 2008, pp. 1096–1103.
- [22] F. A. Gers, J. Schmidhuber, and F. Cummins, "Learning to forget: continual prediction with LSTM," in *International Conference on Artificial Neural Networks (ICANN)*, vol. 2, 1999, pp. 850–855 vol.2.
- [23] A. Vaswani, N. Shazeer, N. Parmar, J. Uszkoreit, L. Jones, A. N. Gomez, L. u. Kaiser, and I. Polosukhin, "Attention is all you need," in *Advances in Neural Information Processing Systems*, vol. 30. Curran Associates, Inc., 2017.
- [24] J. Bromley, J. W. Bentz, L. Bottou, I. Guyon, Y. LeCun, C. Moore, E. Säckinger, and R. Shah, "Signature verification using a "Siamese" time delay neural network," *International Journal of Pattern Recognition and Artificial Intelligence*, vol. 7, no. 04, pp. 669–688, 1993.
- [25] G. Leitmann, "On one approach to the control of uncertain systems," *Journal of Dynamic Systems, Measurement, and Control*, vol. 115, no. 2B, pp. 373–380, 1993.
- [26] J. Shin, T. A. Badgwell, K.-H. Liu, and J. H. Lee, "Reinforcement learning—overview of recent progress and implications for process control," *Computers & Chemical Engineering*, vol. 127, pp. 282–294, 2019.
- [27] F. Schroff, D. Kalenichenko, and J. Philbin, "FaceNet: A unified embedding for face recognition and clustering," in *Proceedings of the Conference on Computer Vision and Pattern Recognition*, 2015, pp. 815–823.
- [28] D. Sheng and G. Fazekas, "A feature learning Siamese model for intelligent control of the dynamic range compressor," in *International Joint Conference on Neural Networks (IJCNN)*, 2019, pp. 1–8.
- [29] D. Angeli, "A Lyapunov approach to incremental stability properties," *IEEE Transactions on Automatic Control*, vol. 47, no. 3, pp. 410–421, 2002.
- [30] M. do Carmo, *Riemannian Geometry*, ser. Mathematics (Boston, Mass.). Birkhäuser, 1992.
- [31] J.-X. Xu, "A survey on iterative learning control for nonlinear systems," *International Journal of Control*, vol. 84, no. 7, pp. 1275–1294, 2011.
- [32] B. R. Barmish, "Necessary and sufficient conditions for quadratic stabilizability of an uncertain system," *Journal of Optimization Theory and Applications*, vol. 46, no. 4, pp. 399–408, 1985.
- [33] D. P. Bertsekas, "On penalty and multiplier methods for constrained minimization," *SIAM Journal on Control and Optimization*, vol. 14, no. 2, pp. 216–235, 1976.
- [34] B. J. Taylor, *Methods and Procedures for the Verification and Validation of Artificial Neural Networks*. Springer Science & Business Media, 2006.
- [35] Y. Tian, K. Pei, S. Jana, and B. Ray, "DeepTest: Automated testing of deep-neural-network-driven autonomous cars," in *Proceedings of the 40th International Conference on Software Engineering*, 2018, pp. 303–314.
- [36] W. Xiang, D. M. Lopez, P. Musau, and T. T. Johnson, "Reachable set estimation and verification for neural network models of nonlinear dynamic systems," in *Safe, Autonomous and Intelligent Vehicles*. Springer, 2019, pp. 123–144.
- [37] W. S. Sarle, "Neural networks and statistical models," in *Proceedings of the Nineteenth Annual SAS Users Group International Conference*, 1994, pp. 1538–1550.
- [38] B. Warner and M. Misra, "Understanding neural networks as statistical tools," *The American Statistician*, vol. 50, no. 4, pp. 284–293, 1996.
- [39] I. Martin-Diaz, D. Morinigo-Sotelo, O. Duque-Perez, and R. D. J. Romero-Troncoso, "Advances in classifier evaluation: Novel insights for an electric data-driven motor diagnosis," *IEEE Access*, vol. 4, pp. 7028–7038, 2016.
- [40] J. Brownlee, *Statistical Methods for Machine Learning: Discover how to transform data into knowledge with Python*. Machine Learning Mastery, 2018.
- [41] M. A. Armstrong, *Basic Topology*. Springer Science & Business Media, 2013.
- [42] A. Paszke, S. Gross, and F. Massa et al., "PyTorch: An imperative style, high-performance deep learning library," in *Advances in Neural Information Processing Systems*, 2019, pp. 8026–8037.
- [43] P. Virtanen, R. Gommers, and T. E. Oliphant et al., "SciPy 1.0: Fundamental Algorithms for Scientific Computing in Python," *Nature Methods*, vol. 17, pp. 261–272, 2020.
- [44] H. I. Freedman, *Deterministic Mathematical Models in Population Ecology*. Marcel Dekker, 1980.
- [45] I. Loshchilov and F. Hutter, "Decoupled weight decay regularization," in *7th International Conference on Learning Representations, ICLR 2019, New Orleans, LA, USA, May 6-9, 2019*. OpenReview.net, 2019.